

Theoretical Trends of Diffusion and Reaction into Tubular Nano- and Mesoporous Structures: General Physicochemical and Physicomathematical Modeling

Christian Amatore*^[a]

Dedicated to the dear memory of the late Pierre-Gilles de Gennes

Abstract: A general and adaptable physicochemical model is presented to evaluate the mass transport within nanopores of mesoporous particles when the mass transport is coupled to heterogeneous kinetics occurring at active sites located onto the nanopore walls surface. The model framework encompasses almost all situations of practical interest in solutions and may be used for characterizing the kinetic rates and constants controlling the system under different sets of experi-

mental conditions. Furthermore, it allows the delineation of simple effective parameters, which should be most useful for optimizing a given material in view of specific applications. For the sake of clarification the simplified model is presented and its results discussed by specializing it for cases

Keywords: adsorption • desorption • diffusion • mesoporous materials • nanopores • nanotubes

where the reactions involve a simple adsorption of a target species on the nanopore immobilized sites as observed for inorganic sponges used in water decontamination. Yet it may easily be extended further to encompass a wider variety of situations where the sites immobilized onto the nanopore walls perform chemical or biochemical transformations as occur in supported catalysis in liquid solution.

Introduction

Synthesis of specific nano- and mesoporous structures decorated by chemically active sites has received increasing attention over the past decade in view of their various applications.^[1–30] The chemical properties lining the pores walls allow the selective loading inside the particles in high concentrations of a target ion or material though this may be present at low concentrations in the external solution. The interest of such properties for filtration, sequestration of desired ions or molecules is extremely high for controlling of the quality of fluids in everyday and industrial applications as well as for environmental purposes, in particular those re-


lated to the secure disposal of dilute radioactive wastes in nuclear plants exhausts of cooling water.

In such applications, the surfaces of nano- or mesopores are lined with highly selective complexation or chelating agents which may readily trap coordinatively any desired species with high efficiency. Note that whenever the corresponding site-target molecular assembly is designed to be reactive chemically or biochemically, the same system may be used as a dispersed catalyst for heterogeneous supported catalysis (see e.g., refs. [13, 14, 18, 19, 26]). Finally, one may even invoke the potential of such structures for the precise and local deliverance of drugs provided that the presence of a target cell or tissue would lead to a specific (e.g., redox, pH) decrease of the complexing or chelating ability of the nanopore surfaces.^[7, 27]

This brief overview of effective and expected applications based on the inorganic “sponges” (see e.g., ref. [17]) concept explains why many synthetic avenues have been explored in order to offer efficiently tailored compact nano- and mesoporous frames decorated by adequate highly complexing ligands or by reactive molecular catalysts.

Until now, most of the works produced in this area have been devoted to the syntheses and experimental testing

[a] Prof. C. Amatore
Ecole Normale Supérieure Département de Chimie
UMR CNRS-ENS-UPMC 8640 “PASTEUR”, 24 rue Lhomond
75231 Paris cedex 05 (France)
Fax: (+33) 1-4432-3863
E-mail: Christian.Amatore@ens.fr

 Supporting information for this article is available on the WWW under <http://www.chemeurj.org> or from the author: Glossary.

mostly driven on empirical views for the most part relying on chemical activity rationales. However, the diffusion-reaction patterns created inside such nano- or mesoporous materials, which allow their cross-communications with the bulk solution, necessarily crucially control the physicochemical efficiency of the systems. This can be understood readily upon recalling that when any characteristic size parameter is made smaller and smaller, the usual ratios between size and surface, on the one hand, and between surface and volume, on the other hand, vary so that surface effects dominate volume ones, and size effects dominate surface ones. This shows that our “macroscopic” chemical knowledge and views may not apply readily and may even lead to wrong considerations.

From the point of view of chemical efficiency only, one wants to decrease the pore diameter sizes, so as to increase their developed lining surface area, and decrease the inert material bulk, that is, the average distance between individual pores. The consequent synthetic purpose is then to reach objects most exclusively formed of nanoscopically folded active surfaces, that is, of particles consisting more or less of hollow volumes framed by dense packing of bundles of nano- or mesotubes separated by thinner and thinner inactive walls, which only goal it is to structure its shape and rigidity. Note that similar materials, that is, with comparable structures are also designed for applications as modern nano-/mesoporous chromatographic phases in chromatographic methods. However, and despite many resemblances in structures and mass-transfer equations governing their functionalities, the chromatographic phase differs from the cases envisioned here in many ways (compare, e.g., ref. [31] for recent important contributions in this area). The main differences stem from the observation that chromatographic phases require weak and reversible interactions between the target species and the nanopore, and involve target species in rather large concentrations. Conversely, here the interactions must be strong and irreversible to result in an efficient sequestration of the species inside the material and must be able to deal with very dilute target species. Another difference is the hydrodynamic regimes of the solutions that contain the porous particles with the consequence that the diffusion layers extending around the particle (see Figure 1b) may differ significantly.

On the other hand, namely, from a physicochemical point of view, decreasing the radius, R_{pore} , of such nanotubes as much as possible with a constant surface area A requires their average length, L , to become infinite compared with their radius: $L = A/(2\pi R_{\text{pore}}) \gg R_{\text{pore}}$. Diffusion within an infinitely long cylinder with a radius not far from molecular dimensions is extremely slow. Indeed, the duration time for a species with a diffusion coefficient D (true one or effective one) to reach the far end of a tube of length L is $T_{\text{diff}} = L^2/D$ (see Supporting Information for Glossary). This affords $T_{\text{diff}} = (A/2\pi R_{\text{pore}})^2/D$, thus establishing that the time delay required to fill up such nanotubes increases drastically upon decrease of their radius. This is even more true because diffusion coefficients prevailing in such nanoscopic structures

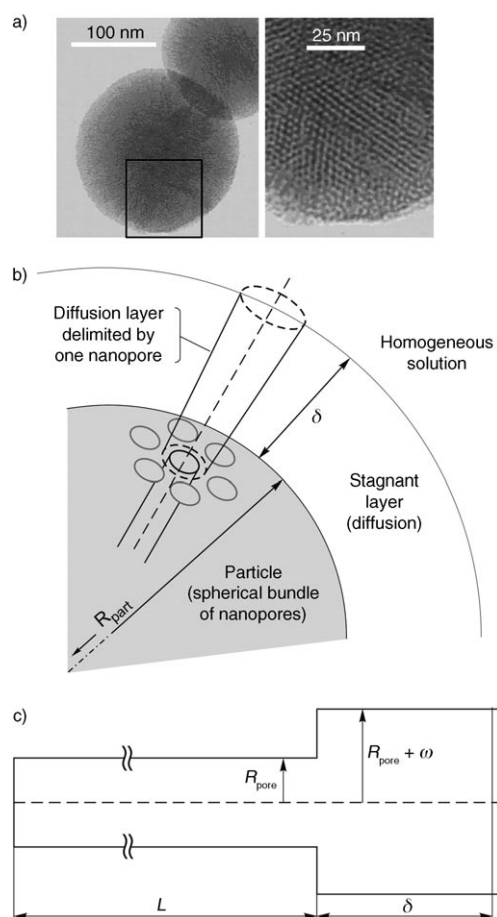


Figure 1. Schematic representation of the general model described here. a) Electron micrographs of spherical sponge particles (left) of a mesoporous silica sample of MCM-41 type;^[17a] the delimited zone is enlarged (right) to emphasize the hexagonal arrangement of nanotubes entrances at the particle surface (courtesy of A. Walcarius, CNRS, UMR 7564, Nancy). b) Sketch of one nanotube connected to its diffusion layer extending into the solution. c) Cross section of b) along the nanotube axis with indication of the geometrical parameters characterizing the system.

may have not the same meaning as those encountered in macroscopic solutions and may then be much smaller than the common ones. In other words, this leads to a physical intrinsic difficulty for a molecule to reach the most inner parts of the active tubes surface, so that the thinner the tube, the lesser it is filled within a reasonable time compatible with a realistic application. Indeed, for a maximum reaction time T_{max} the maximal surface area that may be probed within one nanotube by the target species is about $A_{\text{max}} = 2\pi R_{\text{pore}}(DT_{\text{max}})^{1/2}$ so that it decreases with R_{pore} .

This straight analysis shows that for the physical efficiency one wants to decrease T_{diff} , and therefore keep R_{pore} large enough. This is a conflicting requirement compared with the chemically-based approach, which demands increasing the surface-to-volume ratio of the porous particles. It is then clear that the optimization of such inorganic “sponges” for particular applications has to be accomplished by simultaneously considering the role of their surface chemistry and that related to the physical aspects of their diffusional filling.

It is the aim of this work to provide a first general physico-chemical model allowing the delineation of its main behavioral trends to examine how these dual constraints may be integrated while designing and optimizing an efficient system.

Models

Description of a “sponge” particle as a radial array of meso-

or nanotubes: We assume that the “sponge” material consists of a powder of submillimetric particles (Figure 1a) which are already immersed into a liquid in a batch reactor.^[17a] Since we wish to focus on kinetic matters we assume that at a time taken as the origin ($t=0$), the composition of the liquid in the batch reactor is changed abruptly to contain a total quantity G of a target ion or molecule at concentration C_0^b which the particles should extract ($G=C_0^bV^b$, V^b being the bulk solution volume). We assume for the simplicity of the model that the selectivity of the sites lining particle pores towards this target is unique (namely, that no other competitive extraction may occur) and can be represented by a classical isotherm of adsorption through the intrinsic definition of rate constants of adsorption–desorption to encompass both their possible physical or chemical nature (i.e., involve a transition state or a series of transition states). Indeed, at a constant temperature and pressure the distinction between physical adsorption, chemisorption and covalent binding is irrelevant for the mathematical formulation of our model.

The particles are supposed to be spherical, consisting of a series of radially densely packed cylindrical nano- or mesotubes with thin walls—a situation commonly achieved synthetically with ordered mesoporous silica obtained by the surfactant–template route (see e.g., Figure 1a and b).^[17a] To account for an overall spherical shape when a particle is composed of a dense array of nanotubes, one needs to assume that the tube lengths are not all equal but follow an adequate distribution governed by the growth of particles during the synthesis. Let N_{\max} be the number of tube openings on the outer shell of the particle of radius R_{part} ; $N_{\max} \sim 4(R_{\text{part}}/d)^2$, where πd^2 is the effective surface area required to host one nanopore in the packed array, that is, $d = \gamma(R_{\text{pore}} + \omega)$, where R_{pore} is the inner radius of one nanopore, 2ω the minimum thickness of the inorganic wall separating two adjacent nanopores and γ is a geometric coefficient which depends on the crystallographic arrangement of the array (note that for any array of experimental interest, namely, squared or hexagonal, γ is close to unity so its value needs not to be explicated at this general stage).

To evaluate the average length, L_{av} , of the nanotubes one may rely on a continuous description owing to the very large number of nanopores within a single particle of any practical interest (see Figure 1a and b), though the problem is essentially discontinuous. It is thus shown in Appendix I that $L_{\text{av}} = R_{\text{part}}/3$. Interestingly this number is independent of the respective size and packing arrangement of the nano-

pores compounding the particle provided only that $R_{\text{part}} \gg d$. Conversely, the number Δn_β of nanotubes having a total length $L_\beta = \beta R_{\text{part}}$, that is, comprised between $(\beta - \Delta\beta/2)R_{\text{part}}$ and $(\beta + \Delta\beta/2)R_{\text{part}}$, depends on R_{part}/d and is given by ($0 \leq \beta \leq 1$):

$$\Delta n_\beta = 8 \left[\frac{R_{\text{part}}}{\gamma(R_{\text{pore}} + \omega)} \right]^2 (1 - \beta) \Delta\beta \quad (1)$$

This shows that if one considers constant increments in length, namely, $\Delta\beta = C^{\text{st}}$, the histogram of the lengths distribution is linear irrespective of the geometrical parameters of the array, though the number of nanotubes of each dimension is a function of these geometrical characteristics.

Because in a real experiment one may have distributions of particles sizes and for each particle a distribution of nanopore sizes (see Appendix I), in the following we will focus on a single “nanotube element” as depicted in Figure 1c. Note that such an “element” includes not only the nanotube itself but also the semi-infinite volume of solution delimited by the solid angle concentric with the particle and defined by the overall surface area $\pi\gamma^2(R_{\text{pore}} + \omega)^2$ defined by one nanotube on the particle surface (Figure 1b). Treatment of the activity of a real system consisting of particles containing nanopores having both different sizes may be performed afterwards through statistical averaging considering the experimental R_{pore} and L distributions (see Appendix I). Yet, to systematize and validate this approximation, we first need to examine the physicochemical status of the “external” solution in terms of the spatial repartition of the target species concentration.

Diffusion–convection control around a “sponge” particle placed in solution:

Spherical active particles of any size develop diffusion layers around them. These depend only on the duration of the experiment and on the particle size. This can be rationalized as follows. It is well established that any array of active material (e.g., of ultramicroelectrodes) of much smaller size than that of the overall array develops a series of individual spherical layers centered on each active nanoelement composing the array.^[32] Spontaneous merging of these individual spherical layers creates an effective diffusion layer that contributes to the macroscopic geometry of the array.^[32]

In other words, when applied to the present case, the collective activity of the N_{\max} nanopores opening onto a particle surface generates an overall uniform spherical diffusion layer wrapped around the particle and concentric with it. By virtue of the Nernst–Einstein diffusion law this diffusion layer propagates into the bulk solution at a rate about $(D_{\text{bulk}}/t)^{1/2}$, where t is the time elapsed since the beginning of the experiment, and D_{bulk} the diffusion coefficient of the target species in the solution bulk (note that this is the classical diffusion coefficient so it may differ from that inside the nanopores, see above).

For the sake of reasoning let us assume for now that the particle is performing in a still bulk solution. When the experimental time increases, the thickness of the diffusion layer, $\delta_{\text{diff}} \sim (D_{\text{bulk}} t)^{1/2}$, continuously expands up to the point when it becomes a few times the radius of the particle itself. When this occurs, full radial diffusion imposes that the solution surrounding the particle over a domain of thickness of a few R_{part} behaves under steady state spherical diffusion control. In other words, whenever the solution and particle are absolutely motionless, δ_{diff} extends continuously with time but its maximal extension of importance in controlling the flux to the particle surface is $(\delta_{\text{diff}})_{\text{max}} \sim R_{\text{part}}$.

In a general experiment the whole solution is stirred vigorously to ensure that each individual particle behaves statistically in an identical fashion. Thus, each particle may be considered as being surrounded by a thin stagnant solution layer of thickness δ_{conv} ($50 \mu\text{m} \leq \delta_{\text{conv}} \leq 150 \mu\text{m}$) for common liquids depending on local hydrodynamics).^[33]

Therefore the effective steady-state diffusion layer that expands around each particle cannot exceed $\delta = \min[(\delta_{\text{diff}})_{\text{max}}, \delta_{\text{conv}}]$. This stagnant layer, in which transport occurs exclusively by diffusion, is achieved either through pure diffusion (when $(\delta_{\text{diff}})_{\text{max}} \ll \delta_{\text{conv}}$) or is limited by convection (when $(\delta_{\text{diff}})_{\text{max}} \gg \delta_{\text{conv}}$). This occurs after a time $\Delta t_{\delta} = \delta^2 / D_{\text{bulk}}$,^[33] which is at most a few tens of seconds for realistic systems, that is, much smaller than the usual duration of the particle “filling up” by the target species (see below). Beyond Δt_{δ} the stagnant layer remains stable and the bulk solution, though being continuously depleted, remains homogeneous due either to its vigorous stirring or to the steady state spherical diffusion.

Transport from the bulk solution to a single nanopore entrance: The supply of material into the pore is provided by the steady state diffusion which is quickly reached in the bulk solution. For this reason each nanopore may be treated separately (Figure 1c), so that the overall phenomenon for one particle is obtained by summation over all its individual pores taking into account the distribution of their lengths in Equation (1).

This “external” steady state does not imply that diffusion within a given pore obeys steady state laws, since neither sphericity nor convection may develop within it, yet this ensures that the transfer of matter from the homogeneous bulk solution to the pore entrance adjusts instantly to any moderate change imposed by the nanopore time-dependent activity so that a new steady state is reached instantly by comparison.^[34] This means that at any time of relevance hereafter, the flux of matter which enters a pore through its opening is identical to that which is extracted from the bulk solution by the spherical projection of the circular region consisting of the nanotube and its wall onto the virtual sphere of radius $(\delta + R_{\text{part}})$ surrounding the particle (see Figure 1c). One obtains then the relationship between the average concentration gradients at the entrance of the pore and that prevailing at the end of the stagnant layer:

$$\left(\frac{\partial C}{\partial r}\right)_{r=R_{\text{part}}^+}^{\text{av}} = \frac{1}{\pi R_{\text{pore}}^2} \times \int_{\text{pore entrance}} \int \left(\frac{\partial C}{\partial r}\right)_{r=R_{\text{part}}^+} ds \quad (2)$$

$$= \gamma^2 \left(1 + \frac{\delta}{R_{\text{part}}}\right)^2 \left(1 + \frac{\omega}{R_{\text{pore}}}\right)^2 \left(\frac{\partial C}{\partial r}\right)_{r=R_{\text{part}}+\delta}$$

where the notation $r=R_{\text{part}}^+$ means that the concentration gradient applying over the elementary surface area, ds , of the pore entrance is taken immediately outside the pore. Note that in Equation (2) the superscript “av” means that upon averaging one considers exclusively the nanopore entrance surface area. Indeed, the gradient is null along the margin of the pore entrance (Figure 1c), as this definition allows conserving the overall flux and henceforth compensates automatically the possible flux density variations over the entrance of the pore.

Let us consider now the overall flux of matter over the whole particle surface. For this we consider that in Equation (2) the gradients stand for their mean values averaged over the spherical array of nanopores which delimits the particle surface. Then the variation of the bulk solution concentration, C^b , due to the cumulative activity of N_{part} identical particles, is given at any time by:

$$\frac{dC^b}{dt} = -4\pi D_{\text{bulk}} \frac{N_{\text{part}}(R_{\text{part}} + \delta)^2}{V^b} \left(\frac{\partial C}{\partial r}\right)_{r=R_{\text{part}}+\delta} \quad (3)$$

where V^b is the overall volume of the bulk solution.

On the other hand, owing to the spherical steady state diffusion within the stagnant layer (see Appendix II), one has:

$$\left(\frac{\partial C}{\partial r}\right)_{r=R_{\text{part}}+\delta} = \frac{1}{(1 + \delta/R_{\text{part}})} \times \frac{C^b - C_{R_{\text{part}}^+}^{\text{av}}}{\delta} \quad (4)$$

where $C_{R_{\text{part}}^+}^{\text{av}}$ is the time-dependent average concentration of the target species over the pore entrance. In particular, it follows from Equations (3) and (4) that the differential equation describing the time variation of the bulk concentration is given by:

$$\frac{dC^b}{dt} = -D_{\text{bulk}} \frac{4\pi N_{\text{part}} R_{\text{part}}^2}{V^b} \left(1 + \frac{\delta}{R_{\text{part}}}\right) \times \frac{C^b - C_{R_{\text{part}}^+}^{\text{av}}}{\delta} \quad (5)$$

Note that $4\pi N_{\text{part}} R_{\text{part}}^2$ represents the total active surface area of an ensemble of fully accessible identical particles. Under real conditions, particles follow a distribution of size and some particles may be transiently agglomerated together thus auto-occluding their diffusion layers. So this term may have to be replaced by the accessible surface area of the ensemble of particles at any moment. Yet, we will neglect this feature hereafter since this may be taken into account if necessary.

Equation (5) describes fully the time-dependence of the bulk concentration of the target species. Yet its solution requires an independent knowledge of $C_{R_{\text{part}}}^{\text{av}}$. For this one needs to solve the diffusion–reaction transport inside the nanopore, for which it is advisable to define the problem exclusively within the pore. Combination of Equations (2)–(4) provides the corresponding boundary condition which links the average flux and average concentration at the entrance of the pore:

$$\left(\frac{\partial C}{\partial r}\right)_{r=R_{\text{part}}}^{\text{av}} = \gamma^2 \left(1 + \frac{\delta}{R_{\text{part}}}\right) \left(1 + \frac{\omega}{R_{\text{pore}}}\right)^2 \times \frac{C_{\text{b}} - C_{R_{\text{part}}}^{\text{av}}}{\delta} \quad (6)$$

This condition enables the diffusion–reaction kinetics taking place within the pore to be treated by considering exclusively the phenomena occurring inside the nanopore, C^{b} being a parametric time-dependent variable whose value is regulated in turn by Equation (5). However, one should note that the boundary condition (6) relies on average values of flux and concentration at the pore entrance at any time, and does not link concentration and flux at any given point of the pore entrance. Let us now detail the practical use of such a condition by examining the transport–reaction regime within the nanopore.

Transport and surface sequestration within a single nanopore:

One may envision two main limiting kinetic regimes depending on the inner radius of the pore. When the pore is truly nanometric, that is, has a radius R_{pore} comparable to those of the ion or molecule which it sequesters, the classical diffusion cannot be active since there is no “free” solution for this species to diffuse within. Indeed, under such circumstances the whole solution is submitted to the influence of electrical or physical potentials generated by the pore surface structure. Therefore one has to consider the limiting situation where the pore filling occurs through kinetic exchanges between sites through species released partially within the solution (Figure 2a). Due to its symmetry, the diffusion problem may be treated spatially as a one-dimensional (1D) system where the single space coordinate, x , is the distance from the pore entrance ($x=R_{\text{part}}-r$, so that $x=0$ at the pore entrance and $x=L$ at the far end of the pore).

The other extreme situation to consider is the converse one, namely that in which R_{pore} , though small, remains larger than any ion and molecule dimension. In this case the transport may be described essentially as involving diffusion within a continuum, that is, the solution trapped within the pore, coupled to surface kinetics and site-hopping at the surface of the nanotube (Figure 2a). Due to its symmetry, the system may be treated spatially as a 2D system where the two space coordinates are the distance from the pore entrance along its axis and the radial distance from the nanotube axis.

Yet, before considering this most general case let us examine the 1D-limiting case since this will provide a key to solve efficiently the most general situation. Furthermore, owing to usual geometric requirements in efficient inorganic

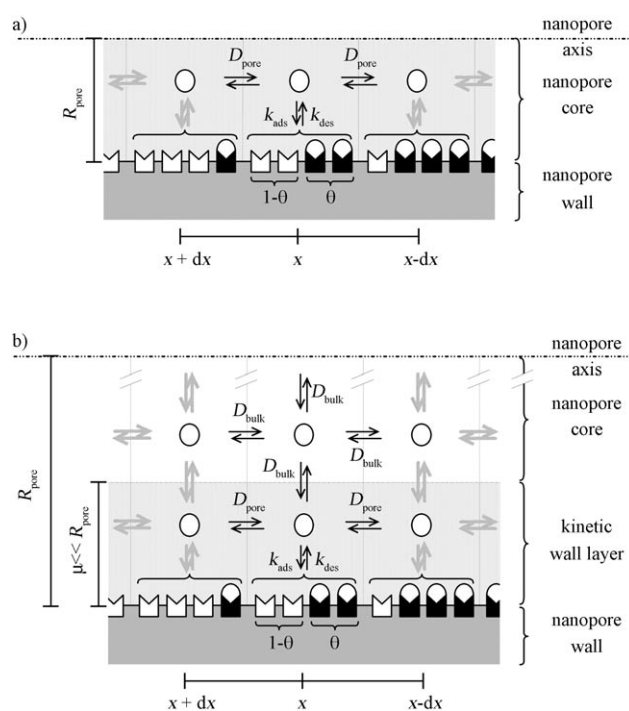


Figure 2. Schematic representation of the two limiting cases considered here. a) Molecular-size nanopore. b) Thin nanopore. See text.

“sponges”, this is presumably the case which prevails under most real conditions of interest.

Formulation of 1D-diffusion-reaction within a nanopore of molecular size:

We consider here a thin nanopore in which the space available to diffusion is at most a few ion or molecule diameters (Figure 2a). Under such conditions it is impossible to define a classical concentration dependence as a function of the radial coordinate. However, one may define a statistically averaged concentration $C^{\text{av}}(x)$ of the target species. This concentration is defined as the infinitesimal number of moles, $d\nu$, of the unbound species (namely, not linked to any site) present in the infinitesimal volume, $\pi R_{\text{pore}}^2 dx$, of an infinitesimal nanopore slice of thickness dx : $C(x) = (d\nu/dx)/(\pi R_{\text{pore}}^2)$. The infinitesimal pore surface area of this slice is $dS = 2\pi R_{\text{pore}} dx$ so that the number of sites (occupied or not) present in the same slice is $d\nu_{\text{sites}} = 2\pi R_{\text{pore}} \Gamma_{\text{site}} dx$, where Γ_{site} is the surface concentration of active sites decorating the nanopore wall. Note that we define here by Γ_{site} merely the maximum surface concentration of the site–target species coverage onto the nanopore walls. In other words, the maximum number (namely at full coverage, that is, after an infinite time, and for a species giving rise to an infinite adsorption equilibrium constant) of moles of target species which may be sequestered by a nanopore is $2\pi R_{\text{pore}} L \Gamma_{\text{site}}$. Let $\theta(x)$ be the local fraction of occupied sites and k_{ads} (in $\text{M}^{-1}\text{s}^{-1}$) and k_{des} (in s^{-1}) be the corresponding rate constants of physical or chemical adsorption and desorption (namely, $k_{\text{des}} = K_{\text{des}} k_{\text{ads}}$, where K_{des} is the desorption equilibrium constant, in M) of the target species onto or from one site. Note that due to the fact that mole-

cules or ions may travel laterally across the nanopore only along distances much smaller than several times their size, the classical Schmoluchowki description of a reaction does not apply here. Also, the nanopore wall chemical composition may generate specific electrostatic potential akin to electric double layers. Therefore, it must be stressed that the physicochemical meaning of the rate and equilibrium constants introduced here, henceforth their values, may substantially differ from those for a classical macroscopic case.

The variation of average concentration within a nanopore slice due to the chemical exchange with the surface during any infinitesimal time duration ∂t at any distance x inside the nanopore is:

$$\left(\frac{\partial C^{\text{av}}}{\partial t}\right)_{\text{surf}} = -\frac{2\Gamma_{\text{sites}}k_{\text{ads}}}{R_{\text{pore}}}[(1-\theta)C^{\text{av}} - \theta K_{\text{des}}] \quad (7)$$

Simultaneously, the unbound target species may diffuse in the solution, so that the second Fick's law equivalent describing the overall behavior of $C^{\text{av}}(x,t)$ is:

$$\frac{\partial C^{\text{av}}}{\partial t} = D_{\text{pore}} \frac{\partial^2 C^{\text{av}}}{\partial x^2} - \frac{2\Gamma_{\text{sites}}k_{\text{ads}}}{R_{\text{pore}}}[(1-\theta)C^{\text{av}} - \theta K_{\text{des}}] \quad (8)$$

Note that D_{pore} , which may drastically differ from D_{bulk} , is formally equivalent to a diffusion coefficient though it has not a classical Nernst–Einstein meaning but a statistical one as in electron-hopping equivalent diffusion.

In the above expression θ is time and space dependent through its dependence on $C^{\text{av}}(x,t)$:

$$\frac{\partial \theta}{\partial t} = k_{\text{ads}}[(1-\theta)C^{\text{av}} - \theta K_{\text{des}}] \quad (9)$$

The system of Equations (8) and (9) defines fully the diffusion-reaction problem within the pore. To be solved, it needs to be associated with a set of initial conditions ($t=0$):

$$0 < x \leq L : C^{\text{av}}(x,0) = 0, \quad \theta(x,0) = 0 \quad (10a)$$

$$x = 0 : C^{\text{av}}(0,0) = C_0^{\text{b}}, \quad \theta(0,0) = 0 \quad (10b)$$

and boundary conditions ($t>0$):

$x=0$ (entrance of pore):

$$\left(\frac{\partial C^{\text{av}}}{\partial x}\right)_{x=0} = -\gamma^2 \frac{D_{\text{bulk}}}{D_{\text{pore}}} \left(1 + \frac{\delta}{R_{\text{part}}}\right) \left[1 + \frac{\omega}{R_{\text{pore}}}\right]^2 \times \frac{C^{\text{b}}(t) - C_{x=0}^{\text{av}}(t)}{\delta} \quad (11a)$$

$x=L$ (bottom of pore):

$$\left(\frac{\partial C^{\text{av}}}{\partial x}\right)_{x=L} = 0 \quad (11b)$$

Note that Equation (11a) follows readily from Equation (6) upon considering the boundary condition inside the pore. This requires a renormalization of the flux to account for the variation of diffusion coefficients on each side of the interface at $x=0$. Equation (11b) expresses simply that the bottom of the nanopore is impermeable to the target species.

Whenever this is of importance, the set of Equations (8)–(11) must be coupled to the rewritten form of Equation (5) to account for the time dependence of the bulk concentration of the target species, namely:

$$\frac{dC^{\text{b}}}{dt} = -D_{\text{bulk}} \frac{4\pi N_{\text{part}} R_{\text{part}}^2}{V^{\text{b}}} \left(1 + \frac{\delta}{R_{\text{part}}}\right) \times \frac{C^{\text{b}}(t) - C_{x=0}^{\text{av}}(t)}{\delta} \quad (12)$$

2D Diffusion-reaction within a single nanopore with thin wall ($R_{\text{pore}} \gg \omega$): When the radius of the pore is much larger than molecular or ionic dimensions the classical 2D-diffusion may be used for the description of transport within the solution which fills the nanotube, namely, for $0 \leq x \leq L$ and $0 \leq \rho \leq R_{\text{pore}}$, where ρ is the radial coordinate measured from the cylindrical nanopore axis, associated to a classical macroscopic formulation of the adsorption–desorption kinetics. Let us denote by $C(x,\rho)$ the concentration at any point of the 2D cross-section of the nanopore along its axis.

By the definition of this case, the physicochemical properties of the thin but nevertheless macroscopic 2D-solution inside the pore are considered akin to those of the bulk. Thus, the diffusion coefficient of the target species is equal to D_{bulk} and a classical diffusion law applies. This affords in cylindrical coordinates:

$$\frac{\partial C}{\partial t} = D_{\text{bulk}} \left[\frac{\partial^2 C}{\partial x^2} + \frac{\partial^2 C}{\partial \rho^2} + \frac{1}{\rho} \frac{\partial C}{\partial \rho} \right] \quad (13)$$

Equation (13) fully defines the problem in the 2D-diffusion zone of the nanopore, but it needs to be coupled to that defining the spatial and temporal dependence of θ . This is written as:

$$\frac{\partial \theta}{\partial t} = D_{\text{site hopping}} \frac{\partial^2 \theta}{\partial x^2} + k_{\text{ads}}[(1-\theta)C(x,\rho) - \theta K_{\text{des}}] \quad (14)$$

to account simultaneously for the adsorption–desorption kinetics and the possibility of “site hopping” interchange through microscopic diffusion as sketched in Figure 2b. Note that $D_{\text{site hopping}}$ is not a classical diffusion coefficient but a parameter equivalent to a diffusion coefficient, which combines microscopic rate constants and diffusion. This formulation compares to that introduced earlier for “diffusion by electron hopping” in redox polymers or redox dendrimers.

The system of Equations (13) and (14) needs to be associated with the following initial conditions ($t=0$):

$$0 < x \leq L, \quad 0 \leq \rho \leq R_{\text{pore}} : C(x,\rho,0) = 0, \quad \theta(x,0) = 0 \quad (15a)$$

$$x = 0, \quad 0 \leq \rho \leq R_{\text{pore}} : C(0,\rho,0) = C_0^{\text{b}}, \quad \theta(0,0) = 0 \quad (15b)$$

and boundary conditions ($t > 0$):

$$0 \leq x \leq L, \quad \rho = 0: \quad (\partial C / \partial \rho)_{\rho=0} = 0 \quad (16a)$$

$$x = L, \quad 0 \leq \rho \leq R_{\text{pore}}: \quad (\partial C / \partial x)_{x=L} = 0 \quad (16b)$$

$$x = L, \quad \rho = R_{\text{pore}}: \quad (\partial \theta / \partial x)_{x=L} = 0 \quad (16c)$$

$$0 \leq x \leq L, \quad \rho = R_{\text{pore}}: \quad \left(\frac{\partial C}{\partial \rho} \right)_{\rho=R_{\text{pore}}} = - \frac{\Gamma_{\text{sites}} k_{\text{ads}}}{D_{\text{bulk}}} [(1-\theta)C - \theta K_{\text{des}}] \quad (16d)$$

$$x = 0: \quad (\partial \theta / \partial x)_{x=0} = 0 \quad (16e)$$

where it must be stressed that although we use the same notations here, in Equation (16d), k_{ads} (in $\text{M}^{-1} \text{s}^{-1}$) and K_{des} (in M) meaning and values are now considered with their usual macroscopic sense. In other words, both parameters include all the microscopic transport along the ρ direction and surface kinetic phenomena which occur within a thin kinetic layer adjacent to the nanopore wall (see Figure 2b). The molecule- or ion-sized thickness, $\mu \ll R_{\text{pore}}$, of this kinetic layer is defined by the fact that at its end (namely, at $\rho = (R_{\text{pore}} - \mu) \sim R_{\text{pore}}$) the physicochemical properties of the solution contained by the nanopore reach their usual macroscopic values.

To complete this formulation, Equations (13)–(16) must be amended by the relationship required to couple the two kinetic regimes taking place in the nanopore to that which prevails in the free solution. Formally, this is given by the set of Equations (17) and (18) which are identical to Equations (11a) and (12) after their appropriate rewriting to take into account the notations used in this section:

$$\left\langle \left(\frac{\partial C}{\partial x} \right)_{x=0} \right\rangle = -\gamma^2 \frac{1}{\delta} \left(1 + \frac{\delta}{R_{\text{part}}} \right) \left(1 + \frac{\omega}{R_{\text{pore}}} \right)^2 \times [C^{\text{b}}(t) - \langle C_{x=0} \rangle] \quad (17)$$

$$\frac{dC^{\text{b}}}{dt} = -D_{\text{bulk}} \frac{4\pi N_{\text{part}} R_{\text{part}}^2}{\delta V^{\text{b}}} \left(1 + \frac{\delta}{R_{\text{part}}} \right) \times [C^{\text{b}} - \langle C_{x=0} \rangle] \quad (18)$$

However, these conditions cannot be used without care. Indeed, they involve two terms, $\langle C_{x=0} \rangle$ and $\left\langle \left(\frac{\partial C}{\partial x} \right)_{x=0} \right\rangle$ which are averaged quantities over the pore entrance surface. So, these equations may be formally applied at a given ρ value in the 2D-domain fraction of the nanopore only when the concentration dependence on ρ at $x=0$ may be neglected. Under our conditions this may be true only when the nanotube wall, ω , is extremely thin compared with R_{pore} , because then the bulk quasi-steady state diffusion layer surrounding the particle penetrates almost unaffected (namely, except for the kinetics occurring at the nanopore wall) inside the nanopore. This simplification is no longer correct when ω is comparable to or even exceeds R_{pore} , because of the strong inhomogeneities of fluxes and concentrations at the pore entrance. When ω is comparable to or even exceeds R_{pore} one

needs to address precisely the diffusional transport problem across the region where the solutions in the diffusion layer and that in the nanopore interact. We therefore need to examine this special situation in a separate section.

Note, however, that this difficulty cancels by definition when the pore radius becomes comparable to molecular and ionic sizes whatever the value of ω/R_{pore} . Indeed, the concentrations and flux in the liquid nanopore may then only be considered as statistically averaged values over the infinitely small action of the pore. So in this situation, whenever steady state conditions apply in the solution surrounding the particle as we consider here, Equations (11a) and (12) may be readily applied at $x=0$. This is why the case of large walls has not been examined in this Section.

Specificities of 2D-diffusion-reaction for a thick-walled nanopore:

As explained above, the geometrical discontinuity involved when the nanopore is not of molecular or ionic size and has simultaneously a thick wall creates extreme flux inhomogeneities in the close vicinity of the pore entrance (namely, over distances that are comparable to ω). On a strict diffusional basis, this problem is indeed akin to that treated previously for recessed electrodes. However, it remains nevertheless original in the sense that the boundary condition created by the presence of a chemically active pore wall differs drastically from that describing an inert pore wall with a recessed electrode at the bottom of the pore. This will be treated elsewhere since it does not affect the diffusional problem per se.

We have shown in our previous work on recessed electrodes^[35] that the large flux variations introduced by the geometrical discontinuities at the pore entrance are filtered readily by diffusion over a distance of a few ω along the pore axis. Thus, one needs only to consider a “buffer” domain located around the pore entrance and extending over a few ω within the free solution or inside the pore. Interestingly, when $\omega/R_{\text{pore}} \rightarrow 0$, the size of this domain vanishes; the “thin-wall” system may then be modeled accurately within the framework elaborated in the previous section.

We have shown in our previous treatment of recessed disk electrode arrays^[35] that formulating the problem with conformal transformations was particularly adequate to suppress the important difficulties introduced by the discontinuities and boundary angles created by the presence of a thick wall. The method consists of transforming the irregular polygon bounding the 2D space in which diffusion occurs into a rectangular 2D space (see Figure 3a). This is performed in two steps, each one involving a specific Schwartz–Christoffel transformation.^[32b,35,36] The first one converts the complex variable $z = \rho + ir'$ (i being the imaginary unit number, $i^2 = -1$, and r' is the coordinate co-directional with r but centered at $r = R_{\text{part}} - L$) into the intermediate one ξ according to Equation (19):^[35]

$$z = f(\xi) = z_{\xi} \int_0^{\xi} \frac{(\xi - \xi_2)^{1/2}}{\xi^{1/2} (\xi - \xi_1)^{1/2} (\xi - \xi_3)^{1-a/\pi}} d\xi \quad (19)$$

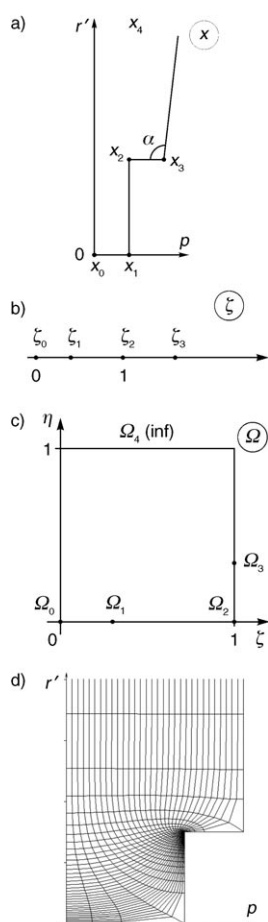


Figure 3. Mathematical treatment by conformal mapping of diffusion within nanopores (see Figure 1c) required when the pore wall thickness, 2ω , is at least of comparable size to the inner diameter of the nanopore $2R_{\text{pore}}$. a) Half-cross-section of the nanopore and its adjacent diffusion layer (see Figure 1b and c) in the real space. b) Effect of the transform $z \rightarrow \xi$ onto a) to generate the half-plane geometry in the ξ space. c) Transform of b) through the application of $\xi \rightarrow \omega$, to produce the closed box equivalent of a) in the Ω space. d) Back-transformation in the real space a) of a uniform rectangular mesh drawn in the closed box c); note that the kinked area near the pore entrance is automatically defined with high precision.

where the variables ζ_1 , ζ_2 and ζ_3 are the images of the poles in the original space labeled x_0 , x_1 , x_2 and x_3 which define the complex positions of the polygon summits in real space (Figure 3a). The angle α gives the average direction of the circular arc describing the particle boundary with the nanopore axis, so that for the experimental cases of interest which involve a dense packing of nanopores $\alpha \sim \pi/2$. Similarly, z_ζ is a scaling complex factor which needs not to be explicated at this stage. The corresponding ζ space is a half-plane (Figure 3b). This is then transformed onto the final closed space $\Omega = \zeta + i\eta$ according to Equation (20):

$$\Omega = \frac{2}{\pi} \Omega_\zeta \arcsin(\sqrt{\zeta}) \quad (20)$$

where again Ω_ζ is an adequate complex scaling factor. As

evidenced in Figure 3c, the Ω space is a closed rectangular box. The interest of the overall transformation $z \rightarrow \Omega$ is readily apparent through the examination of Figure 3d which represents the result in the real space z of an even rectangular grid meshing of the Ω space after its back-transformation $\Omega \rightarrow z$.

This observation is crucial for our purpose here. We have indeed shown previously^[35] that the pattern generated by the sequence of Equations (19) and (20) as exemplified in Figure 3d closely conforms with the real pattern produced by the steady state isoconcentration curves and flux lines. In other words, this shows that except when the sites are extremely reactive (and then only over the very short initial time period required for the active solution to penetrate over a distance of a few ω within the pore) the flux is conserved across this buffer zone.

Thus, provided that the pore length, L , exceeds by far its wall thickness, one may neglect the influence of the distortion caused by the presence of a thick wall, so that the descriptions given in the previous section may be used directly. The relative systematic error thus introduced onto the final quantity of sequestered target is at most of the order of ω/L and concerns only extreme situations where the adsorption/desorption kinetics are faster than diffusion. Since in any real situation of interest one has $L \sim R_{\text{part}} \gg (R_{\text{pore}} + \omega)$ due to the dense packing of nanopores in the particle, it follows that the relative error of the quantities and fluxes of sequestered species is negligible for any real system having an applicative interest.

Owing to our interest here (see Figure 1), this “short pore with thick wall” configuration may then be overlooked. However, it will be fully investigated elsewhere, since it presents several properties of importance for other kinds of applications especially for electroanalysis.

Summary of the models for each limiting case of practical interest:

The different analyses presented above delineate that under any case of real practical importance for the use of nanoporous particles as chemical “sponges” or reactors, the problem of transport and sequestration needs to be treated only within a single nanopore. The outside conditions imposed by the external solution through its steady state layer at the surface of the particle may be replaced by analytical boundaries which govern the relationship between concentration and flux of the target species at the very entrance of the pore.

Diffusion-adsorption within the pore may be treated as a one-dimensional problem when the pore radius is of molecular or ionic size, a situation which simplifies greatly the numerical simulations. However, then the system properties depend on physicochemical parameters (e.g., diffusion coefficient, kinetic rate constants) whose values do not compare at all with usual macroscopic ones. Their values must either be determined independently by molecular Brownian dynamics or be considered as adjustable parameters when fitting simulations to experimental data.

Conversely, when the nanopores, though still nanoscopic, have larger radii, a macroscopic 2D cylindrical formulation may be used. However, when the margin surrounding each pore opening at the particle surface has the size comparable with or larger than R_{pore} , the system cannot be readily uncoupled by considering independently the nanopore and the external solution as may be performed in the treatment of the 1D model as the small-walled 2D model. A proper analysis of transport in this zone was required for connecting the very pore inside to the main part of the diffusion layer around the particle. This showed that a connecting buffer zone extends into the pore and into the external solution only over a few times the size, 2ω , of the inorganic wall that separates two adjacent pores. It follows that, though it may be important for other situations, this cumbersome situation needs not to be considered for any realistic application of such particles as inorganic “sponges” or reactors where $L \gg \omega + R_{\text{pore}}$.

Experimental observables: The particles considered in this study are used experimentally for sequestering a target species from a dilute bulk solution of this species. The particles action will stop when the species coordinated by the active nanopores sites is at equilibrium with the solution filling the nanopores. Note that when the system has reached equilibrium, the target species concentration within the solution filling a nanopore is constant and identical to that of the bulk solution at the end of process. This only ensures the suppression of all chemical and transport fluxes which is the necessary criterion to define the dynamic equilibrium of the system. Let C_{∞}^b be this common concentration.

Irrespectively of the nanopore size, the sites coverage θ_{∞} at equilibrium is:

$$\theta_{\infty} = [1 + (K_{\text{des}}/C_{\infty}^b)]^{-1} \quad (21)$$

so that the overall quantity of species sequestered by one pore reactive sites is:

$$Q_{\infty}^{\text{wall}} = 2\pi R_{\text{pore}} L \Gamma_{\text{site}} \theta_{\infty} = 2\pi R_{\text{pore}} L \Gamma_{\text{site}} / [1 + (K_{\text{des}}/C_{\infty}^b)] \quad (22)$$

Since the amount of target species trapped into the solution filling the nanopore is:

$$Q_{\infty}^{\text{soln}} = \pi R_{\text{pore}}^2 L C_{\infty}^b \quad (23)$$

the overall amount of target species sequestered by a single nanopore is:

$$Q_{\infty} = Q_{\infty}^{\text{wall}} + Q_{\infty}^{\text{soln}} = \pi R_{\text{pore}}^2 L C_{\infty}^b \left[1 + \frac{2\Gamma_{\text{site}}}{R_{\text{pore}}(K_{\text{des}} + C_{\infty}^b)} \right] \quad (24)$$

Noting that the volume and the surface area of a nanopore are proportional to its length L , and taking advantage of

Equations (A1) and (A3) from Appendix I, one obtains for N_{part} identical particles:

$$Q_{\infty}^{\text{tot}} = N_{\text{part}} \left[\frac{4\pi}{3} R_{\text{part}}^3 \left(\frac{R_{\text{pore}}}{d} \right)^2 \right] \left[1 + \frac{2\Gamma_{\text{site}}}{R_{\text{pore}}(K_{\text{des}} + C_{\infty}^b)} \right] C_{\infty}^b \quad (25)$$

On the other hand, the bulk solution has been depleted so that, owing to matter conservation, one obtains the equation giving the value of C_{∞}^b :

$$C_{\infty}^b = C_0^b / \left\{ 1 + \frac{4\pi R_{\text{part}} N_{\text{part}}}{3V_b} \left(\frac{R_{\text{pore}}}{d} \right)^2 \left[1 + \frac{2\Gamma_{\text{site}}}{R_{\text{pore}}(K_{\text{des}} + C_{\infty}^b)} \right] \right\} \quad (26)$$

At any time before the final equilibrium is reached, the overall quantity of the target species sequestered within the particles is equal to that missing from the solution:

$$Q^{\text{tot}}(t) = (C_0^b - C^b)V_b \quad (27)$$

where $C^b(t)$ is given by the solution of the equations defining the 1D or 2D models.

It follows that:

$$Q_{\infty}^{\text{tot}} = (C_0^b - C_{\infty}^b)V_b \quad (28)$$

so that:

$$f(t) = \frac{Q^{\text{tot}}(t)}{Q_{\infty}^{\text{tot}}} = \frac{1 - (C^b/C_0^b)}{1 - (C_{\infty}^b/C_0^b)} \quad (29)$$

defines the fraction of target species sequestered at any time, C_{∞}^b being given by Equation (26).

Analysis of Kinetic Behavior

Dimensionless formulations: The above analysis has provided evidence that the kinetic properties of the systems under investigation depend on several independent parameters. However, the formulations used for the 1D-model or the 2D-model evidence that these parameters play cooperative or antagonist roles in controlling the system behavior, so that a dimensionless formulation presents the advantage of integrating these cumulative effects into a single effective parameter. Actually, this is also important to afford a larger generality of predictions based on simulations. For this reason let us introduce the following dimensionless variables:

$$\text{concentrations : } a = C/C_0^b \text{ or } C^{\text{av}}/C_0^b, c = C^b/C_0^b \quad (30a)$$

$$\text{surface coverage : } \gamma_{\text{site}} = \Gamma_{\text{site}}/(LC_0^b) \quad (30b)$$

$$\text{time : } \tau = D_{\text{bulk}}t/L^2 \quad (30c)$$

$$\text{diffusion coefficients : } \eta = D_{\text{pore}}/D_{\text{bulk}}, \eta_{\text{sh}} = D_{\text{site hopping}}/D_{\text{bulk}} \quad (30d)$$

$$\text{shape parameters : } \sigma = \left(1 + \frac{\delta}{R_{\text{part}}}\right), \psi = \left(1 + \frac{\omega}{R_{\text{pore}}}\right) \quad (30e)$$

$$\text{lengths : } y = x/L, \chi = \rho/R_{\text{pore}}, \varepsilon = (L/R_{\text{pore}})^2 \quad (30f)$$

$$\text{volume : } v = \frac{4\pi R_{\text{part}}^3 N_{\text{part}}}{3V_{\text{b}}} \left(\frac{R_{\text{pore}}}{d}\right)^2 \quad (30g)$$

$$\text{adsorption rate : } \lambda_0 = k_{\text{ads}}L^2C_0^{\text{b}}/D_{\text{bulk}} \quad (30h)$$

$$\text{desorption equilibrium : } \kappa = K_{\text{des}}/C_0^{\text{b}} \quad (30i)$$

$$\text{time constants : } \varphi = \gamma^2\sigma\psi^2(L/\delta), \vartheta = 4\pi N_{\text{part}}R_{\text{part}}^2\sigma L^2/V_{\text{b}}\delta \quad (30j)$$

$$\text{pore storage parameter : } \Xi_0 = \frac{(2\pi R_{\text{pore}}L)\Gamma_{\text{site}}}{(\pi R_{\text{pore}}^2L)C_0^{\text{b}}} = 2\frac{\Gamma_{\text{site}}}{R_{\text{pore}}C_0^{\text{b}}} \quad (30k)$$

where Ξ_0 , the pore storage parameter, compares the maximum quantity of species storable by the nanopore wall sites, namely, $Q_{\text{ads species}}^{\text{max}} = (2\pi R_{\text{pore}}L)\Gamma_{\text{site}}$, to the quantity stored by the solution contained by the nanopore upon considering the initial solution concentration, $Q_{\text{soln species}}^{\text{max}} = (\pi R_{\text{pore}}^2L)C_0^{\text{b}}$. Note that at infinite time, the pore-contained solution has a concentration $C_{\infty}^{\text{b}} = c_{\infty}C_0^{\text{b}}$, so that $\Xi_{\infty} = \Xi_0\left(\frac{C_0^{\text{b}}}{C_{\infty}^{\text{b}}}\right) = \frac{\Xi_0}{c_{\infty}}$ represents the storage parameter after an infinite time.

This set of dimensionless parameters allows recasting the set of equations to afford the dimensionless time-dependent fraction of the sequestered target species. For example, Equation (29) becomes:

$$f(\tau) = \frac{Q^{\text{tot}}(\tau)}{Q_{\infty}^{\text{tot}}} = \frac{1-c(\tau)}{1-c_{\infty}} \quad (31)$$

where c_{∞} is solution of the dimensionless formulation of Equation (26):

$$c_{\infty} = \frac{1-\kappa(1+v)-2v\gamma_{\text{site}}\sqrt{\varepsilon} + \sqrt{(1-\kappa(1+v)-2v\gamma_{\text{site}}\sqrt{\varepsilon})^2 + 4\kappa(1+v)}}{2(1+v)} \quad (32)$$

and $c(\tau)$ is obtained through solving the equations describing the system in each of its limiting cases of experimental interest.

Dimensionless formulation for the 1D limiting problem: Introducing the dimensionless variables defined in Equations (30a)–(30k), the 1D-model mathematical formulation becomes:

$$\frac{\partial a}{\partial \tau} = \eta \frac{\partial^2 a}{\partial y^2} - (\lambda_0 \Xi_0)[(1-\theta)a - \theta\kappa] \quad (33)$$

$$\frac{\partial \theta}{\partial \tau} = \lambda_0[(1-\theta)a - \theta\kappa] \quad (34)$$

and is associated with the following set of initial conditions ($\tau=0$):

$$0 < y \leq 1 : a = 0, \theta = 0 \quad (35a)$$

$$y = 0 : a = C_0^{\text{b}}, \theta = 0 \quad (35b)$$

and boundary conditions $\tau > 0$:

$$y = 0 : \left(\frac{\partial a}{\partial y}\right)_{y=0} = -\frac{\varphi}{\eta}(c - a_{y=0}) \quad (36a)$$

$$y = 1 : \left(\frac{\partial a}{\partial y}\right)_{y=1} = 0 \quad (36b)$$

where the time variations of the bulk solution concentration in Equation (12) are related to that at the pore entrance by:

$$\frac{dc}{d\tau} = -\vartheta(c - a_{y=0}) \quad (37)$$

Dimensionless formulation for the 2D limiting problem:

The mathematical equations which describe the 2D-phenomena occurring inside the nanopore core and those pertaining to its wall surface become in dimensionless formulations:

$$\frac{\partial a}{\partial \tau} = \frac{\partial^2 a}{\partial y^2} + \varepsilon \left(\frac{\partial^2 a}{\partial \chi^2} + \frac{1}{\chi} \frac{\partial a}{\partial \chi} \right) \quad (38)$$

$$\frac{\partial \theta}{\partial \tau} = \eta_{\text{sh}} \frac{\partial^2 \theta}{\partial y^2} + \lambda_0[(1-\theta)a - \theta\kappa] \quad (39)$$

and are associated with the following initial conditions ($\tau=0$):

$$0 < y \leq 1, 0 \leq \chi \leq 1 : a(y, \chi, 0) = 0, \theta(y, 0) = 0 \quad (40a)$$

$$y = 0, 0 \leq \chi \leq 1 : a(0, \chi, 0) = 1, \theta(0, 0) = 0 \quad (40b)$$

and boundary conditions ($\tau > 0$):

$$0 \leq y < 1, \chi = 0 : (\partial a / \partial \chi)_{\chi=0} = 0 \quad (41a)$$

$$y = 1, 0 \leq \chi \leq 1 : (\partial a / \partial y)_{y=1} = 0 \quad (41b)$$

$$y = 1, \chi = 1 : (\partial \theta / \partial y)_{y=1} = 0 \quad (41c)$$

$$0 \leq y < 1, \chi = 1 : \left(\frac{\partial a}{\partial \chi}\right)_{\chi=1} = -\frac{\lambda_0 \Xi_0}{2\varepsilon} [(1-\theta)a - \theta\kappa] \quad (41d)$$

$$y = 0, 0 \leq \chi \leq 1 : \left(\frac{\partial a}{\partial y} \right)_{y=0} = -\frac{\varphi}{\eta} (c - a_{y=0}) \quad (41e)$$

$$y = 0, \chi = 1 : (\partial \theta / \partial y)_{y=0} = 0 \quad (41f)$$

As for the 1D problem, the time variations of the bulk concentration need to be taken into account. It must be realized that a may now vary along the χ coordinate at $y=0$. Yet, within the framework of our 2D model (i.e., $\omega \ll R_{\text{pore}}$), such variations are necessarily slight and are readily filtered by diffusion into the nanopore over a distance $y_{\omega} \sim \omega/L \ll 1$. Therefore, one is allowed to approximate this boundary condition upon considering the mean value of a over the surface of the nanopore entrance, namely:

$$\frac{dc}{d\tau} = -\vartheta (c - \langle a \rangle_{y=0}) = -\vartheta \left(c - 2 \int_0^1 a_{y=0} \chi d\chi \right) \quad (42)$$

Limiting kinetic behaviors: In this section we take advantage of the above dimensionless formulations which allow comparison of the effects of several independent parameters.

For realistic systems one expects the storage parameter Ξ_0 to be extremely large. Indeed, should this parameter be small or not large, the maximum quantity of target species stored in the particle would be comparable to that corresponding to the particle volume filled by the initial solution. In other words, when Ξ_0 is not extremely large the particle action would be akin to emptying the solution by scooping it out physically, a situation which presents no operational gain at all. For this reason, in the following we consider only the realistic case where $\Xi_0 \gg 1$ (note that since the bulk solution concentration necessarily decreases with time, one has then at any instant $\Xi_{\tau} = \frac{\Xi_0}{c^{\text{b}}} \geq \Xi_0 \gg 1$, so that the consideration on Ξ applies at any time).

Similarly, one expects that any adequate site lining of the nanopore walls will have a very low desorption equilibrium constant, that is, $\kappa \ll 1$, though this does not necessarily imply that the irreversible adsorption is fast, namely, that λ_0 is large. Indeed, even when adsorption is efficient and rapid λ_0 may be small since it compares the life-times of adsorption (namely, ca. $t_{1/2}^{\text{ads}} \cong 1/(k_{\text{ads}} C_0^{\text{b}})$) to that of diffusion (namely, ca. $T_{\text{diff}} = L^2/D_{\text{bulk}}$), $\lambda_0 = T_{\text{diff}}/t_{1/2}^{\text{ads}}$.

One-dimensional problem: The system is essentially controlled by Equations (33) and (34). Equation (34) shows that an efficient system requires that either λ_0 or $\lambda_0 \Xi_0 / \eta$ are large for the storage by the wall sites to be non-limiting. Since η is expected to be at most equal to unity [see Eq. (30d)],

$$(\Xi_0 / \eta) \gg 1.$$

Behavior I: When λ_0 is large, both parameters are large so that the adsorption equilibrium is achieved at any place and each instant, namely, $\theta = a/(a + \kappa) \cong 1$. Evidently, this condition cannot hold when $a \rightarrow \kappa$ or when $a < \kappa$; yet, this situation

happens only when $a \rightarrow 0$ and $\theta \rightarrow 0$, so that for our purpose here it can be neglected since it corresponds to a negligible quantity of the target species present either on the wall or in the adjacent solution. To delineate the main behaviors of the system, we will thus consider in the following that provided that λ_0 is large, $\theta \cong 1$ is valid everywhere where $a \neq 0$. Thus, Equation (34) is no more required and Equation (33) becomes:

$$\frac{\partial a}{\partial \tau} = \eta \frac{\partial^2 a}{\partial y^2} \quad (43)$$

which establishes that the target species sequestration within the nanopore is controlled by its diffusion only. We have assumed that steady state diffusion was achieved in the particle diffusion layer. However, this may not be the case inside the nanopore even if by definition $(\delta_{\text{diff}})_{\text{max}} \sim R_{\text{part}} \propto L$. Indeed, since η may be small, on the one hand, the diffusion wave propagates slower inside the nanopore than in the free solution, and, on the other hand, even when $\eta \cong 1$ (see below for the 2D problem), forced convection does not contribute to the transport inside the nanopore. Therefore, it is expected that in realistic situations, the diffusional wave has a time-dependent behavior up to when the end of the nanopore is reached, though diffusion is under quasi-steady state in the diffusion layer surrounding the particle holding the pore.

Conversely, when λ_0 is small, Equation (34) shows that the adsorption kinetics lags behind the diffusional species penetration inside the nanopore.

Behavior II: When $\lambda_0 \gg (\eta / \Xi_0)$ the kinetic term in Equation (33) is very large whenever $(1 - \theta)a > \theta\kappa$. This means that each species penetrating inside the nanopore is ultimately sequestered by its reaction with any still active site. However, where the sites have reached equilibrium, that is, where $(1 - \theta)a = \theta\kappa$, the kinetic term vanishes whatever the values of $\lambda_0 \Xi_0 / \eta$. Hence, a may proceed diffusively inside the pore along the zones where the adsorption equilibrium has been reached, namely, where $(1 - \theta)a = \theta\kappa$ but its progression is stopped as soon as this is not the case and waits up to the moment when saturation is reached due to nearly constant diffusional supply of matter. Only then the kinetic term in Equation (33) may vanish again and the target species is allowed to proceed inside the pore. At a given time, let us consider that for $0 \leq y < y_{\tau}$, the sites are already fully covered (namely, $\theta(y) = a/(a + \kappa) \cong 1$). In other words, the concentration profile of a over the range $0 < y \leq y_{\tau}$ is linear and maintains a quasi-steady state flux which counterbalances the consumption of a at y_{τ} . For $y_{\tau} < y \leq 1$, the solution is empty (namely, $a(y) = 0$) and the wall sites unoccupied (namely, $\theta(y) = 0$). Around y_{τ} , since $(\partial a / \partial \tau)$ cannot be infinite, the large magnitude of the kinetic term is necessarily compensated by a large curvature, namely, a large $|\partial^2 a / \partial y^2|$ value, of the concentration profile. Thus the transition is given by:

$$\frac{\partial^2 a}{\partial y^2} \cong (\lambda_0 \Xi_0 / \eta)(1 - \theta)a \quad (44)$$

By definition of y_τ , $\theta \ll 1$ for $y_\tau < y \leq 1$. So, a good asymptotic approximation of the thickness δ_a of the kinetic layer in which the concentration drop of a occurs is:

$$\delta_a \approx (\lambda_0 \Xi_0 / \eta)^{-1/2} \rightarrow 0 \quad (45)$$

and tends towards zero since $\lambda_0 \gg (\eta / \Xi_0)$.

Behavior III: When $\lambda_0 \ll (\eta / \Xi_0)$ the kinetic term in Equation (33) is also negligible, showing that initially the nanopore fills completely by diffusion [namely, Eq. (43) still applies though for different reasons than before]. Thus, during the first stage, the solution inside the pore diffusively equilibrates with that of the bulk solution. In the second and slower stage, the concentration filling the nanopore inside solution remains equilibrated with that of the bulk at any time, and adsorption proceeds slowly. Thus, the system behaves as if the entire pore wall was fully accessible to the homogeneous bulk solution. So during this second stage the target species sequestration kinetics is commanded only by Equation (34) which simplifies into:

$$\frac{\partial \theta}{\partial \tau} \approx \lambda_0(1 - \theta)c \quad (46)$$

where c is the dimensionless bulk concentration.

The three different kinetic behaviors I–III described above may be conveniently summarized by a kinetic zone diagram upon representing their locations as a function of the values of λ_0 and (Ξ_0 / η) . Note that here we have not considered the situation where $(\Xi_0 / \eta) \leq 1$ since by hypothesis the range of this parameter ought to be limited to its large values. Such diagram is shown in Figure 4a. The qualitative time variations of a/c , θ and $f(\tau)$ in each kinetic zone I–III are represented schematically in Figure 4c assuming that $c = 1$ and $\kappa \approx 0$ (see text and Appendix III).

Two-dimensional problem: As for the 1D situation, we wish to delineate the main kinetic behaviors experienced by the

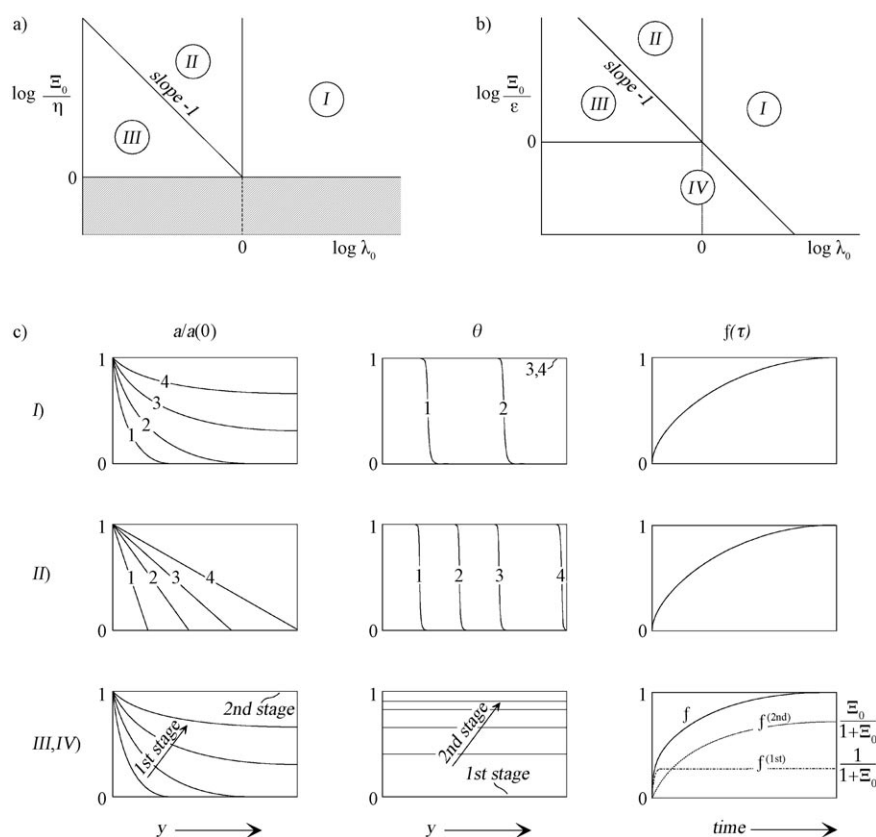


Figure 4. Kinetic zone diagrams illustrating the different behaviors experienced by the system as a function of the main dimensionless parameters which characterize its dynamics: $\lambda_0 = k_{\text{ads}} L^2 C_0^b / D_{\text{bulk}}$, the adsorption kinetic rate, $\Xi_0 = [(2\pi R_{\text{pore}} L) \Gamma_{\text{site}}] / [(\pi R_{\text{pore}}^2 L) C_0^b]$, the storage parameter, as well as of $\eta = D_{\text{pore}} / D_{\text{bulk}}$ and $\epsilon = (L / R_{\text{pore}})^2$. a) 1D problem. b) 2D problem. The qualitative spatial variations of $a/a(0)$, θ and time variations of $f(\tau)$ in each kinetic zone I–III/IV are similar irrespective of the 1D or 2D problem and are represented schematically in c) assuming that $c = 1$ and $\kappa \approx 0$ (see main text and Appendix III). Note that for zone II, in representing $f(\tau)$ the relative proportion between $f_{\infty}^{(1st)}$ and $f_{\infty}^{(2nd)}$ is arbitrary to stress the two-stage behavior. Zone IV exists only for the 2D problem; since this behavior is qualitatively akin to that represented for zone III, it is not particularized in c).

system. For this reason we will neglect here the term η_{sh} since it can be assumed that when the adsorption sites are rigidly anchored to the chemical structure of the nanopore walls any direct exchange between them is negligible compared to the exchange which proceeds through hopping via the solution. Thus, Equation (39) becomes identical to Equation (34), though, the situation is not exactly similar to that identified for the 1D problem because now this is the radial diffusion [namely, the term factor of ϵ in Equation (38) relayed by the coupling Equation (41d)] which commands the supply of species to the walls. Conversely, as for the 1D problem, the axial diffusion term in Equation (38) (namely, $\partial^2 a / \partial y^2$) commands the propagation of the target species within the nanopore.

Though this is not a situation of interest here, the case of wide and short pores (i.e., $\epsilon \leq 1$) corresponds to a fast diffusion of the species inside the nanopore along its axis, so that after a few L^2 / D_{bulk} seconds the nanopore is filled with the target species almost all over its volume except maybe near its wall. Then, adsorption proceeds as described above in the kinetic zone III for the 1D problem (i.e., when $\lambda_0 \ll 1$

and $\lambda_0 \Xi_0/\eta \ll 1$). Due to its peculiarity this situation is not considered anymore in the following and we focus on the system when $\varepsilon \gg 1$, which corresponds to long and thin nanopores, that is, onto the case matching most experimental realistic systems.

Under such conditions the radial diffusion term in Equation (38) necessarily dominates over the axial diffusion term (namely, $\partial^2 a/\partial y^2$) as soon as a radial gradient may build up. Except for the region near the very mouth of the nanopore (see the above discussion in the section on Specificities of 2D-diffusion reaction for a thick-walled nanopore), the only way for a radial gradient component to be forced upon the system is through Condition (41d). This applies at $\chi=1$ and rewrites as:

$$0 \leq y < 1, \chi = 1 : \left(\frac{\partial a}{\partial \chi} \right)_{\chi=1} = -\frac{\lambda_0 \Xi_0}{2\varepsilon} (1-\theta)a \quad (47)$$

for $\kappa \rightarrow 0$. Both terms ε and Ξ_0 are large for the situations of interest herein, so that in contrast to the always large term Ξ_0/η considered above in the 1D problem, the term Ξ_0/ε may take any value depending on the exact system at hand. It follows that $\lambda_0 \Xi_0/\varepsilon$ may achieve also any possible value.

When $\lambda_0 \Xi_0/\varepsilon \ll 1$, except maybe at the very pore entrance, a situation we neglect here, $(\partial a/\partial \chi)_{\chi=1}$ is necessarily negligible because the product $(1-\theta)a$ is at most equal to unity. Whatever is the value of λ_0 , under such conditions the diffusional radial gradient is not able to compete with the axial one. This expresses that the toll imposed by the adsorption kinetics cannot be transferred with significant strength across the nanopore core whatever the value of λ_0 . It ensures that the target species diffuses linearly along the pore axis. So the situation is akin to that considered above in kinetic zone III of the 1D problem (i.e., when λ_0 and $\lambda_0 \Xi_0/\eta$ are both small). During the rapid first stage, the nanopore fills completely through nearly linear diffusion so that the target species concentration becomes equilibrated throughout with that at the pore entrance. In the second and slower stage, kinetics may operate and impose a radial gradient on to the solution whose composition remains independent of y . The situation is then akin to a slow charge transfer case in electrochemistry at a tubular electrode placed into a homogeneous solution [Eq. (46)]. Two main limits are thus found. One when the radial transport to the nanopore wall is fast, namely, the system depends only on the slow heterogeneous kinetics and is governed by the magnitude of λ_0 so that the situation is akin to behavior III met in the 1D problem. In the opposite situation, the adsorption kinetics is faster than the diffusional supply and depletes continuously the target species at the surface.

Then the system kinetics is akin to a Nernstian case, being governed by the radial transport which in turn is imposed by the gradient at $\chi=1$, namely, by $\lambda_0 \Xi_0/\varepsilon$ in Equation (47); this defines a new situation, noted behavior IV (this could not be met in the 1D problem because the radial diffusion was infinite by definition of the 1D model). Comparison between Equations (46) and (47) shows that the relative mag-

nitude of both effects is governed by the ratio: $(\lambda_0 \Xi_0/\varepsilon)/\lambda_0 = \Xi_0/\varepsilon$, behavior III being encountered when $\Xi_0/\varepsilon \gg 1$, while behavior IV is observed when $\Xi_0/\varepsilon \ll 1$. Noting that these two zones: zone III and zone IV, exist only when $\lambda_0 \Xi_0/\varepsilon \ll 1$, it follows that zone III is defined by the area comprised below the segment $\lambda_0 \Xi_0/\varepsilon = 1$ and above $\Xi_0/\varepsilon = 1$, that is, exists only when $\lambda_0 \ll 1$. Zone IV corresponds to the complementary domain located below the axis $\lambda_0 \Xi_0/\varepsilon = 1$ and may be observed whatever the value of λ_0 .

When $\lambda_0 \Xi_0/\varepsilon \gg 1$, $(\partial a/\partial \chi)_{\chi=1}$ in Equation (47) is necessarily large unless the adsorption kinetics are sufficiently fast to reach equilibrium while the species diffuses; indeed, then $[(1-\theta)a - \theta\kappa] = 0$, that is, $\theta = 1$ when $\kappa \ll 1$. Occurrence of the latter condition requires that λ_0 is large. Then the situation is identical to that described above for the 1D problem (kinetic zone I). Conversely, when $\lambda_0 \ll 1$, the kinetics are slow but nevertheless impose an extremely strong toll on the diffusing species through the gradient in Equation (47) because $\lambda_0 \Xi_0/\varepsilon \gg 1$. As for the kinetic behavior II of the 1D problem, where adsorption equilibrium is not yet reached, a is efficiently diverted towards the nanopore wall by its extremely large radial gradient. Therefore, it cannot proceed any deeper within the pore beyond the point y_τ where the local sites have already equilibrated, that is, $a(y) = 0$ for $1 < y < y_\tau$. For $y_\tau < y \leq 0$ the term $(\partial a/\partial \chi)_{\chi=1}$ vanishes locally because $\theta(y) = a/(a + \kappa) \cong 1$. Therefore a may diffuse freely between the pore entrance and the point at y_τ so as to provide the flux which is consumed by the reaction at y_τ . It follows that $a(y) \cong a(0)(1 - y/y_\tau)$ while presenting a negligible dependence on the radial coordinate. This defines the kinetic zone II for the 2D problem.

As for the 1D problem the above limiting kinetic behaviors I–III are best summarized by a zone diagram though this is now a function of λ_0 and (Ξ_0/ε) as shown in Figure 4b. Figure 4c schematizes qualitatively the time variations of a/c , θ and $f(\tau)$ in each kinetic zone I–III assuming that $c = 1$ and $\kappa \cong 0$ (see text and Appendix III).

Conclusion

The above analysis has allowed the delineation of the main trends expected to be achieved when particles consisting of thick bundles of nanopores (see Figure 1) are exposed to a solution with the aim of sequestering and concentrating a dilute target species. Indeed, in such systems adsorption kinetics governs, in fine, the sequestering power but diffusion supplies the dilute species to the active centers lining the nanopores walls. Thus diffusion plays a delicate game which controls the overall activity, thus leading to clearly distinct kinetic behaviors (see Figure 4). To the best of our knowledge the ensuing complexity of the dynamics of such systems has never been considered previously for optimizing their overall behavior or designing them for a special application.

Such particles consisting of an ensemble of densely packed nanotubes are prone to be used for a wide variety of

applications ranging from the sequestration of dilute species as considered here, to supported heterogeneous chemical catalysis or supported enzymatic catalysis. Development of new separating materials for electrophoresis and chromatographic systems may also rely on the same concepts. Indeed, in all such cases, ultimately a kinetic process takes place all along the surface of the nanostructure while diffusion transports the reactant and possible products to and from the active sites and the bulk solution surrounding the particle. So ultimately the overall behavior of any of the above systems will comply in one way or another with the main trends that have been delineated here. Indeed, though adsorption/desorption kinetics considered in this study do not imply an overall transformation of the target species as in catalysis, its physicochemical formulation encompasses all the other cases, except maybe that of enzymatic reactions where Michaelis–Menten limiting kinetics (i.e., $v = v_{\max}$) may be reached. Since the diffusion supply of the target species provides spontaneously a wide range of concentrations inside the reactive nanopore it is then expected that the enzymes located deeper within the nanopore will perform linearly while those closer to the pore entrance may perform in the saturated kinetic region. This may somewhat alter the generic behavior observed in Figure 4 essentially when λ_0 is small while (Ξ_0/ε) or (Ξ_0/η) is large.

Finally, another biological example where the concepts delineated in the above model may find an important application is that of macrophage distribution in blood capillaries when a particular section of a capillary has been activated due to a local infection. Indeed, then the penetration of the macrophages through the capillary wall may be treated as a reaction onto the activated capillary wall section.

For all these reasons we believe that a deeper understanding of the delicate interplay between transport and wall reactivity within nanotubes is required. As evidenced here even for the simplest case of chemisorption the system involves many parameters beyond the main ones which have been considered here (Figure 4a and b) but will ultimately add their specificities onto the overall behavior. To the best of our knowledge this may be treated only through accurate simulations which will be the scope of further works, to be published elsewhere.

In particular, we have explained just above that the case of enzymatic reactors consisting of long nanopores may create poor efficiency due to the specific features of Michaelis–Menten kinetics. It may be advisable to consider shorter and wider pores for such applications. Then the main approximations performed here which allowed a simple outcome (Figure 4a and b) will not be valid anymore. Under such circumstances, the system must be envisioned only as outlined here in the section on Specificities of 2D-diffusion reaction for a thick-walled nanopore, so that its numerical treatment will be eased up by recasting it into its simpler conformal space (see Figure 3).

Appendix

Appendix I: Average length of cylindrical nanotubes packed in a dense array into a spherical particle

Since one nanopore occupies a cross-surface area of πd^2 onto the particle surface the maximum number, N_{\max} , of opened nanotubes is:

$$N_{\max} = \left(\frac{2R_{\text{part}}}{d}\right)^2 \quad (\text{A1})$$

Let us consider the sphere S_n of a smaller radius r_n , inside of the particle and concentric with it, which is crossed over by exactly n nanotubes, so that $4\pi r_n^2 = n\pi d^2$. By definition, these tubes extend at least from the particle surface to the sphere S_n , so that their length, l_n , is at least $l_n = R_{\text{part}} - r_n$. Then one obtains:

$$l_n = R_{\text{part}} \left[1 - \left(\frac{d}{2R_{\text{part}}}\right) n^{1/2} \right] \quad (\text{A2})$$

from where it follows that the average nanotube length, L , in the spherical particle is:

$$L_{\text{av}} = \langle l_n \rangle = \frac{\int_0^{N_{\max}} l_n dn}{\int_0^{N_{\max}} dn} = R_{\text{part}} \left[1 - \frac{d}{3R_{\text{part}}} N_{\max}^{1/2} \right] = \frac{R_{\text{part}}}{3} \quad (\text{A3})$$

On the other hand, rewriting of Equation (A2) gives the number, n_β , of nanotubes having a length βR_{part} ($0 \leq \beta \leq 1$) equal to

$$n_\beta = \left(\frac{2R_{\text{part}}}{d}\right)^2 (1-\beta)^2 \quad (\text{A4})$$

The number Δn_β of nanotubes having a total length $L = \beta R_{\text{part}}$, that is, comprised between $(\beta - \Delta\beta) \times R_{\text{part}}$ and $(\beta + \Delta\beta) \times R_{\text{part}}$, is readily obtained by differentiation of Equation (A4). Thus, one obtains Equation (1) given in the main text:

$$-\frac{\Delta n_\beta}{\Delta\beta} = 8 \left(\frac{R_{\text{part}}}{d}\right)^2 (1-\beta) \quad (\text{A5})$$

which establishes that the histogram of nanopore lengths repartition is a triangle.

This analysis shows that it is sufficient to consider the problem within a single pore, and to perform afterwards an appropriate statistical treatment to take into account the distribution of nanopores according to Equation (A5), and that of particle sizes R_{part} (note that d , representing one chemical constraint, is not supposed to vary for a given type of material). Since the issue of any prediction will be the time variation of a selected parameter \mathfrak{R} , one obtains for one particle of radius R_{part} :

$$\langle \mathfrak{R}_{R_{\text{part}}} \rangle = \frac{\int_0^{N_{\max}} \mathfrak{R}_{R_{\text{part}}}(\beta) dn_\beta}{\int_0^{N_{\max}} dn_\beta} = 2 \int_0^1 \mathfrak{R}_{R_{\text{part}}}(\beta) (1-\beta) d\beta \quad (\text{A6})$$

where $\mathfrak{R}_{R_{\text{part}}}(\beta)$ is the value of parameter \mathfrak{R} predicted at any given time for a nanopore of length $L = \beta R_{\text{part}}$ performing within a particle of radius R_{part} . It then follows that $\langle \mathfrak{R} \rangle$, the predicted experimental value of \mathfrak{R} , as a function of time taking into account the whole distribution is:

$$\langle \mathfrak{R} \rangle = \int_0^\infty \langle \mathfrak{R}_{R_{\text{part}}} \rangle \mathfrak{P}_{R_{\text{part}}} R_{\text{part}} \quad (\text{A7})$$

where $\mathfrak{P}_{R_{\text{part}}} = \frac{dN_{R_{\text{part}}}}{dR_{\text{part}}}$ is the normalized distribution of particles as a function of their radii.

Appendix II

Derivation of Equation (4): Under steady state spherical diffusion, the concentration, C , of any species obeys the steady state form of the second Fick's law:

$$\frac{\partial^2 C}{\partial r^2} + \frac{2}{r} \frac{\partial C}{\partial r} = 0 \quad (\text{A8})$$

where r is the distance from the center of symmetry of the system. It follows readily that:

$$\frac{\partial C}{\partial r} = \frac{\sum_g}{r^2} \quad (\text{A9})$$

where \sum_g is a constant, so that at any distance r (\sum_c is a second constant):

$$C = \sum_c - \frac{\sum_g}{r} \quad (\text{A10})$$

Let C_1 and C_2 be the values of C at any two distances denoted r_1 and r_2 , respectively. Thus:

$$C_1 - C_2 = (r_2 - r_1) \frac{\sum_g}{r_1 r_2} \quad (\text{A11})$$

where \sum_g may be expressed through Equation (A9) at distance r_1 , so that:

$$\frac{C_2 - C_1}{r_1 - r_2} = \frac{r_1}{r_2} \left(\frac{\partial C}{\partial r} \right)_{r=r_1} \quad (\text{A12})$$

Equation (4) derives immediately from Equation (A12) when it is particularized for $r_1 = R_{\text{part}} + \delta$ and $r_2 = R_{\text{part}}$.

Appendix III

Limiting kinetic behaviors for a single nanopore performing in a bulk solution of infinite volume: Our purpose here is only to illustrate the consequences of each limiting behavior I–III/IV which have been evidenced to occur depending on the main parameters which govern the system. For this purpose we wish to provide a rough semiquantitative evaluation of the different kinetic behaviors which may be displayed by the system and are sketched in Figure 4c. For this reason we limit ourselves to the (unrealistic) situation where a single nanopore operates into a solution of infinite volume so that the events occurring within the nanopore do not modify significantly the bulk concentration (namely, $v=0$ and $\vartheta=0$ respectively in Equations (30g) and (30k)). Therefore, here $c(\tau)=1$ at any τ value. Note that the ensuing expressions must then be considered only as asymptotic ones. To be applied to any real circumstances the following results must be convoluted with the time variation of c as documented in sections on Dimensionless formulations and Limiting kinetic behavior. This may alter slightly the limiting kinetic behavior derived below, but the overall trends should remain.

In zone I, or during the first stage of the nanopore filling in zone III, the target species extraction is controlled by its linear diffusion within the pore without appreciable radial diffusion. The situation is similar to that met in chronoamperometry when a planar electrode is placed within a long thin layer cell without convection. Thus the diffusion wave propagates as $\sqrt{\tau}$ except when it meets the bottom of the tube ($y=1$), that is, when $\tau \rightarrow 1$. Therefore, for most of the durations of interest ($\tau < 1$) one has $a(y, \tau) = \text{erfc}(y/2\sqrt{\tau})$. It follows that for a long nanopore, over most of the time:

$$f(\tau) \propto \sqrt{\tau}/(A + \sqrt{\tau}) \quad (\text{A13})$$

where A is a constant close to unity. Thus $f(\tau) \propto \sqrt{\tau}$ while the nanopore fills up but slows down progressively when the bottom of the nanopore is reached (i.e., when $\tau \rightarrow 1$). The limit f_∞ at infinite time of $f(\tau)$ in zone I is unity since both the pore core and its wall sites fill up at the same rate.

When the system is located into zone III the same behavior applies but the nanopore wall sites do not react significantly while the nanopore core solution is filling up. Thus:

$$f(\tau) = f^{(1st)}(\tau) + f^{(2nd)}(\tau) \quad (\text{A14})$$

where $f^{(1st)}(\tau) \propto \sqrt{\tau}$ stands for most of the fast initial stage (solution fills up; see above) while the slow rising function $f^{(2nd)}(\tau)$ corresponds to the second stage (nanopore wall sites react). Note that $f^{(2nd)}(\tau)$ significantly differs from zero only after $f^{(1st)}(\tau)$ has reached its limit $f_\infty^{(1st)} = 1/(1 + \Xi_0)$. The sequestration of the second fraction of the species (namely the main one which is slowly trapped by adsorption onto the wall sites) is given by Equation (34) where now $a=1$ at each instant within the present approximation. At infinite time $f^{(2nd)}(\tau)$ reaches the limit $f_\infty^{(2nd)} = \Xi_0/(1 + \Xi_0)$, so that:

$$f^{(2nd)}(\tau) = f_\infty^{(2nd)} [1 - e^{-\lambda_0 \tau / (1 + \kappa)}] = \frac{\Xi_0 [1 - e^{-\lambda_0 \tau / (1 + \kappa)}]}{1 + \Xi_0} \quad (\text{A15})$$

In zone IV (which is relevant only to the 2D problem), the same applies except for the exponential argument in Equation (A15) which is proportional to Ξ_0/ϵ .

In zone II, the situation is quite different. The analysis developed for this case (see main text) shows that the diffusional wave moves relatively fast but that the adsorption kinetics inclines it to every point where the wall sites are not yet filled up. Therefore a sharp front of propagation is created at $y=y_r$. Whenever $0 < y < y_r$, a varies linearly with y and does not depend significantly on the radial coordinate. Across this zone, $\theta=1$, while beyond a vanishingly small distance δ_a after y_r [see Eq. (45)] $a = \theta=0$ for $y_r < y < 1$.

Establishing the precise kinetics of $f(\tau)$ in this zone requires simulations due to the nonlinearity of Equation (44). However, one may estimate its general behavior based on scaling factors. Indeed, the above analysis showed that $a(y) = a(0)(1 - y/y_r)$ whenever $0 < y < y_r$. Thus, $a(y_r) \propto a(0)/y_r$ due to the linear decrease of the gradient while y_r increases with time. Thus, one has from Equation (46):

$$\frac{\partial \theta}{\partial \tau} \approx \lambda_0 (1 - \theta) [a(0)/y_r] \quad (\text{A16})$$

So the time duration $d\tau$ necessary for filling up the ring located at y_r and having a surface area $dA = 2\pi R_{\text{pore}} dy_r$ is:

$$d\tau \propto y_r dy_r / [\lambda_0 a(0)] \quad (\text{A17})$$

On the other hand, when the wave reaches y_r , a surface $2\pi R_{\text{pore}} y_r$ of the pore wall is completely filled up and a volume $\pi R_{\text{pore}}^2 y_r$ of the nanopore core is half filled up. Thus, $f = (\Xi_0 + 1/2)/(\Xi_0 + 1)y_r$, that is, $f \approx y_r$ since $\Xi_0 \gg 1$. It then follows from Equation (A16) that:

$$f df \propto \lambda_0 a(0) d\tau \quad (\text{A18})$$

Owing to our purpose in this Appendix, we again neglect the variations of $a(0)$, so that:

$$f \propto \sqrt{\lambda_0 \tau} / (A' + \sqrt{\lambda_0 \tau}) \quad (\text{A19})$$

which shows that f keeps again a diffusional-type behavior though this is commanded now kinetically, namely, by the magnitude of λ_0 and not by a Nernst–Einstein diffusion coefficient.

Acknowledgements

This work has been supported in part by CNRS, ENS and UPMC (UMR 8640). The author wishes to express his thanks to Prof. I. Svir (CNRS and KNURE) as well as to Drs. A. Oleinick and O. Klymenko

(KNURE) for their important and helpful comments and suggestions while this theory was developed. Dr. A. Walcarius (CNRS) is also greatly acknowledged for thoughtful discussions at the initial stage of this work and for providing the EM photographs shown in Figure 1a.

- [1] a) C. T. Kresge, M. E. Leonowicz, W. J. Vartuli, J. S. Beck, *Nature* **1992**, 359, 710; b) J. S. Beck, S. B. McCullen, J. B. Higgins, J. L. Schlenker, J. C. Vartuli, W. J. Roth, M. E. Leonowicz, E. W. Sheppard, *J. Am. Chem. Soc.* **1992**, 114, 10834; c) J. C. Vartuli, D. H. Olson, E. W. Sheppard, K. D. Schmitt, C. T. Kresge, W. J. Roth, M. E. Leonowicz, J. L. Schlenker, *Chem. Mater.* **1994**, 6, 2317; d) J. C. Vartuli, C. T. Kresge, M. E. Leonowicz, A. S. Chu, S. B. McCullen, I. D. Johnson, E. W. Sheppard, *Chem. Mater.* **1994**, 6, 2070; e) J. S. Beck, J. C. Vartuli, G. J. Kennedy, C. T. Kresge, W. J. Roth, S. E. Schramm, *Chem. Mater.* **1994**, 6, 1816; f) H. Yang, G. A. Ozin, C. T. Kresge, *Adv. Mater.* **1998**, 10, 883; g) H. Yang, N. Coombs, G. A. Ozin, *J. Mater. Chem.* **1998**, 8, 1205; h) W. J. Hunk, G. A. Ozin, *Chem. Mater.* **2004**, 16, 5465.
- [2] J. Wu, A. F. Gross, S. H. Tolbert, *J. Phys. Chem. B* **1999**, 103, 2374.
- [3] a) H. Wakayama, Y. Fukushima, *Chem. Mater.* **2000**, 12, 756; b) T. Itoh, K. Yano, T. Kajino, S. Itoh, Y. Shibata, H. Mino, R. Miyamoto, Y. Inada, S. Iwai, Y. Fukushima, *J. Phys. Chem. B* **2004**, 108, 13683; c) H. Wakayama, Y. Fukushima, *Ind. Eng. Chem. Res.* **2006**, 45, 3328; d) I. Oda, K. Hirata, S. Watanabe, Y. Shibata, T. Kajino, Y. Fukushima, S. Iwai, S. Itoh, *J. Phys. Chem. B* **2006**, 110, 1114.
- [4] S. Han, K. Sohn, T. Hyeon, *Chem. Mater.* **2000**, 12, 3337.
- [5] B. J. Scott, G. Wirnsberger, G. D. Stucky, *Chem. Mater.* **2001**, 13, 3140.
- [6] a) J.-S. Lee, S. H. Joo, R. Ryoo, *J. Am. Chem. Soc.* **2002**, 124, 1156; b) M. Choi, F. Kleitz, D. Liu, H. Y. Lee, W.-S. Ahn, R. Ryoo, *J. Am. Chem. Soc.* **2005**, 127, 1924.
- [7] J.-H. Sun, Z. Shan, T. Maschmeyer, M.-O. Coppens, *Langmuir* **2003**, 19, 8395.
- [8] P. V. Braun in *Nanocomposite Science and Technology* (Eds.: P. M. Ajayan, L. S. Schadler, P. V. Braun), Wiley-VCH, Weinheim, **2003**, pp. 155–214.
- [9] M. C. Burleigh, M. A. Marcowitz, S. Jayasundera, M. S. Spector, C. W. Thomas, B. P. Gaber, *J. Phys. Chem. B* **2003**, 107, 12628.
- [10] S. H. Kim, B. Y. H. Liu, M. R. Zachariah, *Langmuir* **2004**, 20, 2523.
- [11] L. A. Villaescusa, A. Mihi, I. Rodrigues, A. E. Garcia-Bennett, H. Miguez, *J. Phys. Chem. B* **2005**, 109, 19643.
- [12] C. Sanchez, B. Julian, P. Belleville, M. Popall, *J. Mater. Chem.* **2005**, 15, 3559.
- [13] M. Hartmann, *Chem. Mater.* **2005**, 17, 4577.
- [14] F. Hoffman, M. Cornelius, J. Morell, M. Froeba, *Angew. Chem.* **2006**, 118, 3290; *Angew. Chem. Int. Ed.* **2006**, 45, 3216.
- [15] C.-F. Cheng, H.-H. Cheng, P.-W. Cheng, Y.-J. Lee, *Macromolecules* **2006**, 39, 7583.
- [16] Y. Wang, F. Caruso, *Chem. Mater.* **2006**, 18, 4089.
- [17] a) A. Walcarius, C. Delacôte, *Chem. Mater.* **2003**, 15, 4181; b) A. Walcarius, E. Sibottier, M. Etienne, J. Ghanbaja, *Nat. Mater.* **2007**, 6, 602; c) M. Etienne, A. Quach, D. Grosso, L. Nicole, C. Sanchez, A. Walcarius, *Chem. Mater.* **2007**, 19, 844.
- [18] a) Z. Koinya, V. F. Puentes, I. Kiricsi, J. Zhu, J. W. Ager III, M. K. Ko, H. Frei, G. A. Somorjai, *Chem. Mater.* **2003**, 15, 1242; b) R. Nakamura, H. Frei, *J. Am. Chem. Soc.* **2006**, 128, 10668; c) H. Han, H. Frei, *Microporous Mesoporous Mater.* **2007**, 103, 265; d) W. Wasylenko, H. Frei, *J. Phys. Chem. C* **2007**, 111, 9884.
- [19] a) M. K. Kidder, P. F. Britt, Z. Zhang, S. Dai, E. W. Hagaman, A. L. Chaffee, A. C. Buchanan III, *J. Am. Chem. Soc.* **2005**, 127, 6353; b) M. K. Kidder, P. F. Britt, A. L. Chaffee, A. C. Buchanan III, *Chem. Commun.* **2007**, 52.
- [20] X. Ji, P. S. Herle, Y. Rho, L. F. Nazar, *Chem. Mater.* **2007**, 19, 374.
- [21] S. Bhattacharya, K. E. Gubbins, *Langmuir* **2006**, 22, 7726.
- [22] A. Sayari, Y. Yang, *Chem. Mater.* **2005**, 17, 6108.
- [23] H. M. Alsayouri, J. Y. S. Lin, *J. Phys. Chem. B* **2005**, 109, 13623.
- [24] C. Lei, Y. Shin, J. Liu, E. J. Ackerman, *J. Am. Chem. Soc.* **2002**, 124, 11242.
- [25] B. Coasne, A. Galarneau, F. D. Renzo, R. J. M. Pellenq, *Langmuir* **2006**, 22, 11097.
- [26] A. Zimmerman, J. Chorover, K. W. Goynes, S. L. Brantley, *Environ. Sci. Technol.* **2004**, 38, 4542.
- [27] A. Vinu, M. Miyahara, K. Ariga, *J. Phys. Chem. B* **2005**, 109, 6436.
- [28] a) R. Hernandez, H.-R. Tseng, J. W. Wong, J. F. Stoddart, J. I. Zink, *J. Am. Chem. Soc.* **2004**, 126, 3370; b) T. D. Nguyen, Y. Liu, S. Saha, K. C.-F. Leung, J. F. Stoddart, J. I. Zink, *J. Am. Chem. Soc.* **2007**, 129, 626.
- [29] X. Gao, S. Nie, *J. Phys. Chem. B* **2003**, 107, 11575.
- [30] W. Shui, J. Fan, P. Yang, C. Liu, J. Zhai, J. Lei, Y. Yan, D. Zhao, X. Chen, *Anal. Chem.* **2006**, 78, 4811.
- [31] a) A. Cavazzini, F. Gritti, K. Kaczmarek, N. Marchetti, G. Guiochon, *Anal. Chem.* **2007**, 79, 5972; b) F. Gritti, W. Piatkowski, G. Guiochon, *J. Chromatogr. A* **2003**, 983, 51; c) K. Miyabe, G. Guiochon, *J. Phys. Chem. B* **2002**, 106, 8898.
- [32] a) C. Amatore, J.-M. Savéant, D. Tessier, *J. Electroanal. Chem.* **1983**, 147, 39; b) C. Amatore, *Electrochemistry at Ultramicroelectrodes in Physical Electrochemistry: Principles, Methods and Applications* (Ed.: I. Rubinstein), Marcel Dekker, New York, **1995**, Chapter 4.
- [33] C. Amatore, S. Szunerits, L. Thouin, J.-S. Warkocz, *J. Electroanal. Chem.* **2001**, 500, 62.
- [34] C. A. Amatore, M. R. Deakin, R. M. Wightman, *J. Electroanal. Chem.* **1986**, 207, 23.
- [35] C. Amatore, A. I. Oleinick, I. Svir, *J. Electroanal. Chem.* **2006**, 597, 77.
- [36] M. A. Lavrientiev, B. V. Shabat, *Methods of Complex Function Theory*, Science, Moscow, **1973**.

Received: October 15, 2007
Published online: April 22, 2008